Evaluation of Source-Term Data for

Plutonium Aerosolization

Los Alamos

An Affirmative Action/Equal Opportunity Employer

Evaluation of Source-Term Data for
Plutonium Aerosolization

John M. Haschke

MASTER

EVALUATION OF SOURCE-TERM DATA
FOR PLUTONIUM AEROSOLIZATION

by

John M. Haschke

ABSTRACT

Relevant data are reviewed and evaluated in an effort to define the time dependence and maximum value of the source term for plutonium aerosolization during a fuel fire. The rate of plutonium oxidation at high temperatures is a major determinant of the time dependence. Analysis of temperature-time data for oxidation of plutonium shows that the rate is constant $(0.2$ g PuO_2/cm^2 of metal surface per min) and independent of temperature above 500°C. Total mass and particle distributions are derived for oxide products formed by reactions of plutonium metal and hydride. The mass distributions for products of all metal-gas reactions are remarkably similar with approximately 0.07 mass% of the oxide particles having geometric diameters $\leq$ 10 μm. In comparison, 25 mass% of the oxide formed by the PuH_2+O_2 reaction is in this range. Experimental values of mass fractions released during oxidation are evaluated and factors that alter the release fraction are discussed.

INTRODUCTION

A broad spectrum of concerns are associated with the transportation of special nuclear materials. An accident scenario of interest is the possible dispersion of plutonium-containing particles into the environment if a shipping container for plutonium metal or a reactive plutonium compound is involved in a fuel fire. Reliable estimates of the hazards posed by such a plutonium release are contingent on the availability of technical data to define the source term for

aerosolization of plutonium oxide particles. Although several
studies of plutonium aerosolization by burning metal are
reported,[1-5] essential data are undefined. Information
pertinent to plutonium release during self-sustained oxidation
of plutonium has recently been reviewed and evaluated,[6] but
the concerns addressed in that assessment differ significantly
from those created by an external fire.

The aerosolization source term for the incident outline
above varies during the course of the fire. The formation of
aerosolizable particles from the non-aerosolizable metal is a
complex process characterized by three distinct stages. The
release probability and the source term are zero for a period
of time during which the container temperature remains below
the 640°C melting point of plutonium and the integrity of the
container is preserved. The source term becomes non-zero when
the container is breached by highly corrosive molten
plutonium. Whereas most refractory metals such as Ti, V, Ta
and W have limited solubilities in liquid plutonium[7] and are
breached rather slowly, other metals such as steel readily
form low-melting intermetallic phases[7] and are more rapidly
breached. During this second stage, the source term increases
with time as liquid metal progressively escapes from the
container and reacts to form particles of plutonium oxide.
The rates of these processes determine the length of time
required to convert the metal to oxide, and the rate at which
the source term increases from zero to a constant maximum
value marked by complete oxidation. During the third stage
the source term is invariant and defined by the total quantity
of plutonium oxide and the aerosolizable fraction of that
product. The maximum theoretical amount of oxide may not be
dispersed because of kinetic limitations; the length of time
to approach that point is very incident specific.

This report addresses important factors for defining the
time dependence of the source-term and its maximum value for
the scenario of interest. These factors are the oxidation
kinetics of plutonium metal and plutonium hydride at

2

temperatures up to 1000°C, the particle distribution of products formed by those reactions and the kinetics of processes limiting entrainment of particles. Since some of the required information is divergent or unavailable, the conclusions of this report are based on a broad spectrum of literature describing fundamental and engineering studies and in certain cases rely on the use of interpolation, extrapolation and modeling.

FUNDAMENTAL PROPERTIES

Pertinent Physical and Chemical Properties

Plutonium is a reactive metal exhibiting complex properties and forming stable compounds with most other elements. The unalloyed metal has six allotropic forms between room temperature and its melting point at 640°C.[8] Differences in hardness and other properties are observed for each phase. Unalloyed plutonium, often described as "alpha phase," is a hard metal existing at room temperature. Since this form of Pu is only stable up to 122°C, the alpha phase is not actually present at the temperatures of interest. The delta phase is a malleable metal normally existing in the 315 to 457°C range, but this form occurs over a wide temperature range when plutonium is alloyed with gallium. The delta-phase alloy containing approximately 1 mass% Ga is stable when cooled to room temperature.

Plutonium forms two oxides, Pu_2O_3 and PuO_2. These friable crystalline phases are thermodynamically stable; their respective free energies of formation at 25°C are -378 and -238.5 kcal/mol.[9] Pu_2O_3, the lower-composition equilibrium product formed during oxidation of plutonium metal, is readily converted to PuO_2 in air. This conversion is so facile that only PuO_2 is observed on the surface of the metal under 500 torr O_2 at temperatures up to 500°C.[10]

Plutonium forms a complex series of hydrides in the composition range bounded by PuH_2 and PuH_3.[11] The cubic di-

3

hydride structure readily accommodates additional hydrogen, and a continuous solid solution forms between PuH_2 and PuH_3 as the temperature and hydrogen pressure are varied. The free energies of formation of PuH_2 and PuH_3 at 25°C are -31.2 and -40.4 kcal/mol, respectively. The hydrides are pyrophoric crystalline materials that react violently to form PuO_2 upon exposure to air.

The sizes of product particles formed by the $Pu+O_2$ and $Pu+H_2$ reactions are strongly dependent on the reaction temperature. Whereas all oxide particles formed at low temperature are 5 μm or less in size,[12] particles with diameters exceeding 3 mm are formed at temperatures above 500°C.[1] In a parallel way, the hydride obtained near room temperature is a fine powder and that formed at temperatures above 300°C contains centimeter-sized particles.[13] Possible origins of this temperature dependence are discussed in the next section.

Oxidation Mechanisms

An understanding of the physical processes associated with oxidation of plutonium metal and hydride provides a basis for evaluating data relevant to source-term evaluation. The oxidation behavior of metal by air and oxygen is well defined and pertinent references are cited in recent reports.[10,14] Plutonium oxidation is a "paralinear" process involving three stages shown by the curve in Figure 1. If a clean metallic surface is exposed to oxygen, the extent of the ensuing reaction follows a functionality characteristic of a diffusion-controlled process. As the thickness of the adherent oxide layer increases on the metal surface, the rate of oxygen diffusion through that layer decreases according to a parabolic curve like that observed for stage I in Figure 1.

The formation of oxide particles begins during stage II. The second stage is characterized by a linear reaction extent-time curve with a slope that defines the constant oxidation rate. At the onset of stage II, the thickness of the adherent

product layer attains a critical value determined by the buildup of stress induced by forming low-density oxide (molar volume = 23.67 cm^3/mol) on the high-density metal (molar volume = 12.20 cm^3/mol). This stress is relieved by cracking and spalling of the oxide layer. Localized enhancement of the reaction rate occurs at spallation sites. As the oxide thickness increases at these reactive sites, the resulting decrease in rate is offset by spallation and rate enhancement at other sites. This process establishes a constant average layer thickness and a constant bulk reaction rate. Stage III is a similar linear process entered after a transition period, but the origin of this change is unknown.

Variations observed in the sizes of product particles from Pu+O_2 and other Pu+gas reactions with temperature are consistent with the spallation mechanism described above. The observed increase in particle size with increasing reaction temperature is interpreted as a combination of two factors. The first of these is variation of metal hardness and malleability with temperature. Hardness data for the allotropes of plutonium show a progressive decrease with each phase transition and a five-fold difference in the hardness value for alpha and delta phases.[15] The increasing malleability of plutonium with temperature reduces the stress generated at the product-metal interface and promotes formation of a thicker product layer before spallation occurs. Data for several actinide metal + hydrogen reactions indicate that formation of centimeter-sized hydride particles occurs if the reaction temperature equals or exceeds half the melting temperature of the metal in degrees centigrade.[13]

A second factor that may alter product particle size is kinetic in nature. Spallation of particles via a stress cracking process involves nucleation of cracks at the surface and propagation of those cracks through the stressed material with ultimate coalescence and formation of free particles. Nucleation and propagation are both time-dependent, and the time period available for their occurrence is important in

determining particle size. Although the temperature
dependence of spallation is unknown, the activation energies
are probably small compared to the E_a of 33 kcal/mol for stage
II oxidation.[10] Consequently, the growth rate of the oxide
layer is large compared to the spallation rate at high
temperatures and formation of large particles is favored. At
room temperature the oxide growth rate is extremely slow and
the longer time available for spallation favors extensive
crack formation and small particle sizes. Since the
activation energy for Pu+H$_2$ is low (E_a = 2.0 kcal/mol)[13] and
the hydriding rate at room temperature is 10^6 times faster
than the rate for Pu+O$_2$,[16] hydride products should contain
larger particles than the oxide formed at the same
temperature. Whereas the largest particle diameter observed
for low-temperature hydride is near 100mm,[17] that for low-
temperature oxide is approximately 5 μm.[12]

The oxidation of plutonium hydride is a secondary
reaction for which little change in particle size is
anticipated. The molar volume of PuO$_2$ is virtually identical
to that for PuH$_2$ (23.17 cm^3/mol) and minimal stress should
exist at the oxide-hydride interface. This rationale leads to
the conclusion that the particle size distributions for the
hydride reactant and oxide product should coincide.
Experimental observations do not support this conclusion. The
count mean diameter (1.5 μm) measured for the oxide product of
the PuH$_2$+O$_2$ reaction[18] is noticeably shifted relative the mean
value (5.0 μm) for the hydride[17] and the BET (Brunauer,
Emmett, Teller) surface area of the sample increases by a
factor of 3 to 5 during oxidation.[19]

The spallation mechanism occurring during hydride
oxidation apparently involves a physical process other than
interface stress produced by reactant-product mismatch. The
observed decrease in particle size is consistent with a
conceptual fracture mechanism based on fundamental properties
of oxide and hydride. During oxidation, the thermodynamically
stable chemical arrangement does not involve release of

6

gaseous hydrogen, but its adsorption to form a higher-stoichiometry hydride within the PuH_2-PuH_3 solid-solution region of the phase diagram.[11] As the PuO_2 layer forms on the surface of a particle, the product hydrogen dissolves in the residual hydride center of the particle. This process continues until the stoichiometry of the hydride core approaches the PuH_3 limit. Additional hydrogen cannot be absorbed or readily escape through the thick oxide layer. The resulting increase in internal pressure leads to particle fragmentation.

Oxidation Kinetics

The oxidation of plutonium proceeds through several stages, but all of them do not have equal impact on the source term. As shown in Figure 1, completion of the parabolic process and onset of spallation occurs after 3 h at 300°C and 1 torr oxygen pressure. The time span of stage I decreases with increasing temperature and oxygen pressure and is not a major factor in determining the onset of particle spallation at temperatures above 640°C and at the 160 torr O_2 partial pressure of the atmosphere. Consequently, only stages II and III need be considered for establishing the time dependence of the source term.

The anticipated kinetic behavior of the Pu+O_2 reaction at temperatures of interest is shown by Arrhenius curves in Figure 2. Solid segments of the curves show the oxidation rate, K, in mg O_2/cm^{2}min measured for stages II and III at 500 torr O_2 pressure and temperatures up to 450°C.[10] Extrapolations of the temperature trends established by the data are shown by the dashed segments. The changes in slope correspond to transitions from low-temperature processes having activation energies of 19 kcal/mol to high-temperature processes having higher E_a values of 33 and 46 kcal/mol for stages II and III, respectively. As shown by Figure 1, the transition from stage II to stage III occurs after an extended time period and the later stage may not be entered during the

time frame of a fire. K is also dependent on the O_2 pressure, P, and varies as P^n. Below 400°C, K is rather insensitive to P with $0 \leq n \leq 1/3$. Above 400°C, n = 1/2 for stage II and n = 1 for stage III.

The extrapolated rate curves in Figure 2 provide a basis for predicting oxidation rates for $Pu+O_2$ in air at elevated temperatures. Even for n = 1, the pressure correction from 500 to 160 torr O_2 reduces K by approximately a factor of two and is considered negligible. For stage II, a 40 s time period is calculated for completely oxidizing a 1 kg Pu sphere in air at 1000°C, and half of a 200 g Pu cylinder should react in about 30 s at 850°C. This prediction stands in sharp conflict with an experimental observation by Stewart showing that 115 g of a 200 g cylindrical sample remained unreacted after 23 min in a fuel fire at 860°C.[1] Possible origins of this discrepancy include: (a) error in the experimental observation (b) depletion of the oxygen concentration in the fuel fire atmosphere near the sample and (c) a change in oxidation mechanism that invalidates the Arrhenius extrapolation.

The validity of the experimental observation is seen by comparing oxidation rates derived from data reported by Stewart[1] with values obtained from similar data reported by Mishima.[3] Relevant data extracted from time-temperature curves are presented in Table I with average oxidation rates calculated for each test. The results obtained from Stewart's data are shown by solid symbols in Figure 2 and those from Mishima's data are shown by open symbols. Error limits in the rate are based on estimated uncertainties in reaction times and sample surface areas. Three significant results are evident: (a) the oxidation rates are in agreement, but slower than predicted by Arrhenius extrapolation, (b) the rates are independent of temperature in the range above 500°C and (c) the rates for unalloyed metal and gallium-containing alloy are indistinguishable. Although oxidation rates measured for various Ga-containing alloys in air at room temperature are a

factor of 10 to 100 less than that for unalloyed plutonium,[20] the oxidation rates of these metals appear to converge at a temperature near 500°C.[21] The average oxidation rate for plutonium at temperatures above 500°C is 0.16±0.08 g PuO_2/cm^2min.

The rate results provide insight into the potential effects of oxygen depletion during a fuel fire. Use of the square-root pressure dependence for the stage II rate shows that the O_2 pressure at the sample must be reduced to about 0.5 torr in order to produce the apparent reduction in rate at 860°C. Not only does this pressure seem inordinately low and improbable, but the possibility of kinetic control by oxygen depletion is virtually precluded by the other set of kinetic results. The oxidation rates for reaction in a fuel fire[1] are identical to those for self-sustained burning in flowing air that provided a twenty-five-fold excess of O_2.[3]

The existence of reducing conditions in a fuel fire merits further evaluation. Volatilization and cracking of hydrocarbons produce a non-oxidizing atmosphere. However, a significant fraction of the fuel must also burn in order to maintain a 1000°C flame temperature. High concentrations of H_2O, CO_2 and CO must be present in the fire. Reactions of these species with plutonium are thermodynamically favored and are expected to occur at the temperature of the flame. For example, the reported[22] oxidation rate of delta-stabilized plutonium by water vapor at 15 torr pressure and 500°C equals that for alloy oxidation by O_2 at 500 torr and 500°C.[10]

Although a definitive explanation is not possible for the rate behavior of $Pu+O_2$ above 500°C, a change in reaction mechanism provides the most reasonable interpretation. Three possibilities merit consideration. The first involves formation of a progressively thicker oxide layer on the metal with increasing temperature. This explanation is unlikely because the thickness increase must precisely compensate for the temperature-driven increase in transport rate across the layer. A particle size increase with temperature is not

evident above 500°C. An alternate possibility is the self-limiting nature of autothermic chemical reactions.[23] A limit on the rate of a self-sustaining reaction arises because thermal acceleration ceases when the point is reached where the rate of heat loss balances the rate of heat production. Since the sample temperature cannot increase beyond this point, a limiting condition and a constant rate are achieved. Further evaluation of this concept is needed to determine if autothermic control is operative. The most likely explanation for the constant rate is a gas phase transport limitation occurring for gas mixtures. Removal of oxygen from the gas at the gas-solid interface produces a layer of nitrogen and other unreactive gases at the surface. The oxidation rate is controlled by the transport of oxygen or oxygenated species across that layer.

A constant oxidation rate for plutonium at temperatures above 500°C is unexpected and inconsistent with conclusions described in a recent review.[6] According to earlier interpretations of experimental data, the rate of $Pu+O_2$ at high temperatures is altered by metal type, sample mass and temperature, but the data in Table I do not support these conclusions. The recommended burn rate of 180 g/h for plutonium does not recognize the well-established dependence of rate on the surface area of metal,[10,20] and cannot be reconciled with the observed oxidation of a 1.8 kg Pu sample in 55 min.[3] The value cannot be compared with the 0.2 g PuO_2/cm^2min rate derived in this work or applied to a specific situation. Although the mathematics of source term calculation during the time-dependent period is simplified by the existence of a constant oxidation rate, definition of the oxide quantity present at a given point in time is complicated by lack of information about metal release rates and geometries of molten metal deposits formed during failure of containment vessels.

The oxidation of high-surface-area plutonium hydride is a two-stage process.[19] The initial stage is extremely rapid

10

with a negative activation energy (E_a = -2.1 kcal/mol) suggesting that the oxidation rate is determined by the adsorption of O_2 on the surface. During this stage a diffusion barrier of oxide advances toward the centers of the hydride particles and leads to a comparatively slow second stage of reaction. This is a constant-rate process over time and has E_a = 10.0 kcal/mol. Incomplete oxidation is observed at low temperatures in experiments conducted over the 50 to 360°C range at 10 torr O_2 pressure.

The kinetics of $PuH_2 + O_2$ are altered by several factors. Increasing the reaction temperature dramatically increases the fraction of hydride consumed during the initial processes. Whereas only 20% of the hydride reacts in the initial rapid stage at 100°C, the hydride is totally oxidized via this process at temperatures above 400°C. At 10 torr O_2 pressure the first stage is complete within minutes.[19] The pyrophoric nature of the hydride powder formed at temperatures below 100°C is well documented and different from that of the coarse product obtained at temperatures above 300°C.[24] The low-temperature hydride ignites and burns spontaneously when exposed to air; the high-temperature product only ignites in air when heated to 270°C. Rapid and complete oxidation of either product is expected if a hydride container is breached and the shipment is exposed to a fuel fire.

SIZE DISTRIBUTIONS

Size Distribution Data for the Product of $Pu + O_2$

Size distribution data for the product of metal oxidation are essential for source term definition. Although particle size measurements are described by various workers, distributions are only reported for selected fractions, not for an entire oxide product. Whereas the particle size distributions of products from Pu+gas reactions are strongly temperature dependent up to 500°C, data for products obtained above 500°C suggest that thermal effects on size are minimal.

Derivation of a total distribution for high-temperature oxide
necessitates the combination of size distributions for large
and small particles. This combination process is accomplished
using distribution data for products of other Pu+gas reactions
to correlate separate distributions of oxide particles.

Cumulative mass distributions for large particle
fractions formed by high temperature oxidation are reported by
Stewart[1] and by Mishima.[2] The log-normal distributions of
geometric particle diameters measured by Stewart for the
fractions not entrained by the up-draft in fuel fire
experiments are shown in Figure 3. Data for the residue
obtained at 860°C (solid circles) are in good agreement with
those for a 500°C product (open circles), but only the second
distribution accounts for the entire oxide mass. As shown by
solid triangles, a partial distribution[2] of an unentrained
oxide residue formed by combustion in flowing air at
temperatures up to 560°C is in good agreement with those for
fuel-fire tests.

The curve defined by solid symbols in Figure 4 shows the
cumulative particle distribution measured by Mishima[3] for an
oxide fraction entrained by an air flow of 5.25 m/sec (11.7
mph). The sample was collected during self-sustained
combustion of a 1.8 kg metal sample at 925°C. The data
provide a uniquely detailed picture of particle dimensions in
the micron and submicron size range, but their contribution to
the total distribution of oxide particles is unknown.

Essential information for deriving a total distribution
for the oxide is obtained by evaluating particle size data
reported for products formed by reactions of plutonium with
other gases. The cumulative particle distribution for
plutonium hydride is derived from a distribution for powdered
plutonium metal.[17] The metal was initially prepared by
hydriding massive plutonium at room temperature and then
thermally decomposing the hydride in vacuum to regenerate the
metal.[13] Since the BET surface areas of the hydride and metal
powders are identical and invariant after repeated hydride-

12

dehydride cycles, the geometric particle size distribution measured for the metal is adopted for the hydride. The cumulative particle size data obtained from the distribution presented by Stakebake[17] are listed in Table II with size-mass fraction data calculated for spherical particles with the stated geometric diameters. The resulting cumulative mass distribution for the hydride is shown by open triangles in Figure 3. A renormalized cumulative particle distribution for hydride sizes less than 10 μm is shown by open circles in Figure 4.

Several aspects of the size distributions in Figure 3 are important in defining a total distribution for plutonium oxide. Key features of the curves are their shapes and their regions of coincidence. The total mass distributions for oxide and hydride are defined by two linear segments implying bimodel distributions of particles in both products. Whereas the dimensions of the largest oxide particles are about 1 mm, the largest hydride particles are about 0.1 mm in size. This difference in large particle sizes contrasts sharply with the remarkably close agreement observed for all distributions in the size range below 50 μm. These features appear to be characteristic of the distributions for products of all Pu+gas reactions, not a fortuitous coincidence. Small particles with similar sizes might be formed during spallation processes that produce dissimilar large particles. Regardless of the basis for this coincidence, it suggests that distribution data for the hydride might be used as a guide for reconstructing a total distribution for high-temperature oxide formed by Pu+O$_2$.

Additional insight is gained from a parallel examination of the particle distributions in Figure 4. Although the resolution of particle fractions is much less for hydride than for oxide, the agreement observed between the curves suggests that the coincidence of particle sizes beginning near 50 μm is maintained into the submicron range. The count mean diameter (1.3 μm) for hydride particles $\leq$ 10 μm is in close agreement with that (1.2 μm) for the entrained oxide. The small

difference appearing at the upper end of the distribution may
occur because the tubular collection apparatus used by
Mishima[3] for sampling the airborne fraction tends to exclude
particles with large diameters.[25] The observed coincidence of
distributions suggests that hydride data can be substituted
for oxide data in the small particle range.

Derivation of a meaningful total mass distribution for
plutonium oxide requires that the distribution for large and
small particles be combined without skewing the result. A
reasonable approach is suggested by examining the mass
distributions data for hydride in Table II and that for oxide
in Figure 3. A small fraction (0.2%) of the hydride mass
appears in the 15 μm cumulative fraction and 1.8% of the mass
is included in the 30 μm cumulative fraction. A comparable
amount (1.2%) of the mass is included in the 32 μm fraction of
oxide residue. The two distributions may be combined by
substituting the 30 μm cumulative mass fraction of hydride for
the 32 μm cumulative mass fraction of the oxide.

The total mass distribution derived for high-temperature
PuO_2 by the substitution method is presented in Table III and
Figure 5. Comparison of the total distribution with the
partial distribution in Figure 3 shows that all features of
the oxide data are reproduced by the composite curve. Greater
detail in the definition of small particle sizes is achieved
by redistributing the 1.5 μm fraction for the hydride in
accordance with Mishima's data in Figure 4. The accompanying
particle distribution in Table III is based on a spherical
particle assumption.

Size Distribution Data for the Product of $PuH_2 + O_2$

Size distributions of oxide particles produced by
oxidation of plutonium hydride are described in studies by
Edison et al.[4,5] and by Stakebake and Robinson.[18] Using the
results of an extensive investigation of several Pu+gas
reactions involving air, a mixture of gases designed to
simulate combustion products of organics, H_2, an $H_2 + N_2$ mixture

14

and H_2 followed by air exposure, Edison et al. conclude that the respirable particle fraction produced by exposing hydride to air is not significantly different from the fractions produced by other Pu+gas reactions. In earlier work, Stakebake and Robinson observed that oxidation of the hydride by air is accompanied by substantial particle size changes and by an increase in surface area.[18] This behavior is consistent with the pyrophoric nature of the hydride and the results reported by Stakebake and Robinson are selected as the basis for defining the size distribution of oxide formed from hydride.

The particle size distribution measured by Stakebake and Robinson[18] for the PuH_2+O_2 product is shown by the open symbols in Figure 6. Although 95% of the particles are included in the 8 μm cumulative fraction, the distribution of larger particles is undefined. As evidenced by comparing typical mass and particle distributions in Tables II and III, a substantial fraction of the mass usually resides in the largest 5% of the particles. The particle distribution given in Table IV is obtained by assuming that the linear log-normal particle distribution applies to particle sizes in excess of 8 μm. The accompanying mass distribution in Table IV is derived using a spherical particle assumption. The log-normal mass distribution defined by these data is shown by open symbols in Figure 7.

Size Distribution Modeling of Secondary Products

Extrapolation of the particle distribution for the $Pu+O_2$ product beyond the 95% cumulative fraction seems insignificant, but the potential impact on the mass distribution is substantial. The largest 5% of the particles accounts for 80% of the oxide mass. The derived mass distribution is strongly dependent on extrapolated data and the second linear segment suggesting a bimodal mass distribution (cf. Figure 7) is based solely on extrapolation. A model for describing the fragmentation of reactant particles

during a secondary reaction like PuH_2+O_2 is developed in an effort to independently predict the product size distribution.

In concept, the fracture model applies a fixed fragmentation pattern to reactant particles having a known distribution and constructs a new distribution for the product. The basic assumption for defining the fragmentation pattern is that each spherical reactant particle with diameter d fractures to form new spherical particles. As shown by a two-dimensional section through a reactant sphere in Figure 8, the fragmentation pattern is defined by a closest-packed planar array of spheres with diameters d_1, d_2, and d_3 having magnitudes of 0.33 d, 0.13 d, and 0.05 d, respectively. The reactant sphere is approximated by adding an identical layer above and another below the initial array and by filling peripheral recesses on the upper and lower surfaces with d_2 spheres. Each reactant sphere produces 21 d_1 spheres, 30 d_2 spheres and 18 d_3 spheres. Since this composite array fills only 82% of the original sphere volume, the residual volume is distributed proportionally among the three fractions such that 91.65% of the volume or mass of the original sphere appears as d_1 spheres, 8.12% appears as d_2 spheres and 0.23% appears as d_3 spheres. Each individual mass fraction in the reactant distribution is reassigned according to these percentages. The new mass distribution is generated by categorizing and summing the product masses in appropriate fractions.

Mass and particle distributions derived for the PuH_2+O_2 product using the fracture model are presented in Table V. These results are based on the size distribution for PuH_2 in Table II after the 1.5 μm fraction was repartitioned to define a 0.5 μm fraction containing a mass fraction of 3.0×10^{-9}. The fracture model was applied to hydride particles with sizes $\geq$ 15 μm. Masses of particles with sizes $\leq$ 8 μm were combined with those of new fragments to generate the mass distribution in Table V. The corresponding particle distribution is based on spherical particle assumption.

16

The effectiveness of the fracture model in predicting size distributions of secondary reaction products is evidenced by evaluating the results for PuH_2+O_2. The merits of the model are demonstrated by the correspondence of measured (open circles) and predicted (solid circles) particle distributions in Figure 6. A parallel comparison of the mass distributions is shown in Figure 7. The agreement is somewhat surprising. Whereas the count mean diameter measured by Stakebake and Robinson[18] is 1.5 μm, that predicted by the model is 1.9 μm. A bimodal mass distribution is also predicted and the mass fraction existing in the large particle distribution corresponds well with that derived by extrapolation of the experimental particle distribution. An additional evaluation is made by calculating the increase in surface area during reaction and comparing the anticipated increase with the three-fold to five-fold change observed during oxidation.[19] As expected, the calculated areas for spherical particles are 10 to 20 times less than the experimental BET values, but fragmentation according to the model produces a 2.9 fold increase in surface area. Closer agreement between the observed and predicted quantities would be achieved by fracturing all particles and by forming larger particles through failed fracture in a small percentage of cases.

THE RELEASED FRACTION

Comparison of Observations

The mass fraction of oxide lost from a particle source is described in the literature[1-6] by a variety of terms that carry a spectrum of connotations. The terminology used by Mishima[3] seems most consistent with the focus of this report. The material removed from the source by entrainment in the existing draft is described as the "released fraction".

Experimental values of the released fraction are based on measurements of the plutonium quantity entrained by gases flowing over the metal during oxidation. The experimental

conditions of various studies are diverse and cannot be compared on a common basis. This situation may be advantageous because data from a spectrum of conditions helps to establish a range of values that might be anticipated. The comparison of empirical released fractions with particle size data is a complex issue. Since size measurements of released fractions have maximum geometric dimensions approaching 10 μm,[3] this diameter provides a reasonable limit for entrainment and is adopted for evaluating data in this report.

Measurements of released fractions are described in several reports. In two early experiments by Stewart,[1] plutonium samples placed on a stainless steel mesh were burned in the up-draft of a fuel fire at temperatures up to 900°C. Additional test conditions are listed in Table I. The released fractions obtained from the differences between the initial masses and those collected in a tray below the sample are 0.01 and 0.03. However, as shown in Table I, the corresponding fractions are 0.002 and 0.008 when based on the masses of plutonium determined by integration of deposition contours. In a later publication,[26] the author concludes that a mass fraction of 0.001 is a conservative estimate of the dispersal.

Tests by Mishima[3] were conducted with ignited metal samples in the forced up-draft of a collection apparatus. Conditions of these studies are also presented in Table I. Results are reported as release rates with values in the 4.5×10^{-3} to 3.2×10^{-2} mass%/h range. However, Mishima's data provide a basis for evaluating the released fraction. Since particle collection times for two experiments are shorter than the time periods required for complete oxidation of the metal, the quantities of oxide present during collection must be calculated as a basis for evaluating the released fraction. In all cases, zero time for oxidation and collection are assumed to coincide. The amounts of oxide formed during the collection periods are defined by the length of collection, the sample surface area and the oxidation rate

(0.2 g PuO_2/cm^2min). The resulting released fractions in Table I are in good agreement and suggest that significant differences do not exist between the behavior of alloyed and unalloyed plutonium.

Results of an extensive set of release experiments are described by Edison et al.[4,5] who studied the metal+gas reactions of delta-stabilized plutonium and alloys of plutonium with iron and uranium at 450°C. Gaseous reactants are those noted in the preceding discussion of particle size data for PuH_2+O_2. The mean released fraction determined for Pu, Pu-Fe alloy and Pu-U alloy with all gaseous reactants are 0.00021, 0.00055 and 0.00038, respectively. Evaluation of release data for all metals with H_2, simulated organic combustion mixture and H_2+N_2 mixture yield average released fractions of 0.00026, 0.00032 and 0.00026, respectively. Similar analyses of data for reaction of Pu-Fe and Pu-U alloys with air and for reaction of all metals with H_2 followed by air exposure give released fractions of 0.00050 and 0.00076, respectively. The global average released fraction of 0.00038 obtained from the tests by Edison et al.[5] agrees with the 0.00027 value obtained from the results of Mishima.[3]

The mass distribution derived for the product of Pu+O_2 is consistent with the measured released fractions. As shown by Figure 5, the 10 μm cumulative particle size encompasses a mass fraction near 0.0007. This fraction is a factor of two larger than the empirical values from Mishima[3] and from Edison et al.[5] and is considered to represent the maximum entrainable fraction for oxide formed by high-temperature oxidation of plutonium.

Fundamental properties of stress-driven spallation reactions are implied by the observed agreement of released mass fractions for all Pu alloy+gas reactions and the coincidence of mass and particle distributions shown in Figures 3 and 4. The products of spallation reactions at high temperatures have bimodal mass distributions and the distributions of small particles are remarkably similar

regardless of gaseous reactant or size distribution of the large particles. These observations suggest that formation of large particles is the fundamental spallation process and that formation of small particles is a consequence of that process. An analogy can be drawn to breaking a piece of chalk. The dust and fines formed during breakage are characteristic of the fracture process, not of the sizes of the two chalk pieces formed by the fracture. The bimodal distribution and the characteristic size distribution of small particles vanish as the sizes of the large particles decrease to the point that their dimensions equal those of small particles formed during fracture. This situation is realized for the fine plutonium oxide powder produced by air oxidation at room temperature.

Particle size and released fraction data for PuH_2+O_2 are not in agreement. Although Edison and coworkers[4,5] conclude that the respirable fraction of the product formed by reaction of hydride with air is not significantly different from those of other metal+gas reactions, the mass distribution derived from data reported by Stakebake and Robinson[18] in Figure 7 shows that the 10 μm cumulative fraction is 0.25. The average released fraction (0.00076) derived from the results of Edison et al.[5] is smaller by a factor of thirty-three.

Evaluation of test observations reported by Edison et al.[5] for PuH_2+air shows that the results are inconsistent with known properties of the hydride and suggest that the experimental procedures were flawed. The hydride formed at the 450°C reaction temperature is a coarse product with a low surface area and non-pyrophoric nature.[13] In certain cases, the products of the $Pu+H_2$ reaction had retained the shape of the metal samples. In several instances, hydrides not exposed to air changed color from black to green during cooling under argon flow. This color change is characteristic of PuO_2 formation and suggests that a layer of Pu_2O_3 formed during hydriding was further oxidized during cooling. Hydride surfaces were undoubtedly passivated by an oxide layer prior

20

to air exposure. At the flow rates and times of the experiments, a 1 ppm level of contamination by O_2 or other oxygenated species in the gas stream would convert 0.2% of a typical sample to oxide. Sparking and spallation were observed in one case with a Pu-Fe hydride and in another instance with a Pu-U hydride; the released fractions were 0.0046 and 0.10, respectively. Since the observations by Stakebake and Robinson[18] are consistent with properties anticipated for hydrides in shipment, their data are recommended for source term definition of oxide formed by the PuH_2+O_2 reaction.

The Release Process

The maximum release fraction is in principle a precisely defined point on a size distribution, but substantial variation is observed. Experimentally determined released fractions for $Pu+O_2$ bracket the anticipated value. Results of laboratory tests are a factor of two less than predicted by the 10 μm point; results of fuel fire tests far exceed that value. Since these differences remain after correction for the quantities of oxide present during collection, other possible origins for their occurrence merit examination.

The velocity of air flow over the oxide source is a factor that should contribute to the observed variability in released fraction. Entrainment differences are anticipated for the 525 cm/s flow velocity used by Mishima[3] and the 40 cm/s flow velocity used by Edison et al.,[4,5] but are not evident in the measured fractions. The effect may be masked by the influence of other factors. The magnitudes of draft velocities in fuel fires should be evaluated and their effect on the source term should be more adequately defined.

Other factors altering the released fraction are less readily identified and quantified. These factors include physical blockage of the oxide source from the air flow by large oxide particles and by other objects in the vicinity. A related factor is the tenacious adherence of small oxide

particles to larger fragments.[2] The importance of entrainment
is seen in the high released fractions measured by Stewart.[1]
The experimental design was such that each oxide particle was
unavoidably entrained in the up-draft after it spalled.
Particles with dimensions approaching 30 μm were apparently
dispersed by the fire. The likelihood of entraining such
large particles from a surface source is certainly much lower
than from a source placed on a mesh several feet above the
burning fuel.

The conditions simulated by Stewart's tests[1] do not
represent a credible scenario. Molten metal is not expected
to remain suspended in the up-draft for an extended period of
time and significant particle spallation is not expected
during that period. At the high-temperature oxidation rate
for Pu+O$_2$, molten metal must remain suspended for
approximately 3.5 min in order to form a product layer having
a thickness equal to the 0.6 mm median mass diameter observed
for high temperature oxide particles. Stewart's measurements
lead to a substantial over-estimation of the released fraction
and their use for source-term definition must be accompanied
by appropriate caution.

The effects of several factors described above are
apparent in the released fractions listed in Table I.
Although Mishima[3] conducted all experiments at the same air
velocity and the results are corrected for oxide formation,
the released fractions are strongly dependent on the
collection time. A graph of the data in Figure 9 shows a
linear dependence of released fraction on the length of
collection. As defined by the slope, the released fraction
changes by 5 x 10^{-6} per minute until the maximum value is
reached. The concept of a release rate has been employed by
Mishima,[3] and further evaluation of this idea seems to hold
merit.

Release rates derived from experimental data are
surprisingly consistent. The collection intervals used for
rate calculations are corrected for the fact that, on the

average, only half of the oxide is present during the
formation period or during the collection period if it is less
than the formation period. The effective intervals for the
sequence of three tests based on Mishima's data[3] in Table I
are 75, 23, and 11 min and the corresponding release rates are
6.2, 7.8, and 10.9 μg PuO_2/gPuO_2 min. The magnitudes of these
rates decrease with increasing collection time and their order
is reverse of that for released fractions suggesting that the
release rate is not constant with collection time, but
diminishes as the release fraction approaches its maximum.
The average release rate (5 μg PuO_2/PuO_2 min) defined by the
slope of the curve in Figure 9 is recommended.

CONCLUSIONS

Experimental data form the basis for defining size
distributions and release fractions for plutonium oxide
sources in fuel fires. However, the relevance of test
conditions to those of interest must be evaluated in light of
chemical and physical properties of plutonium metal, plutonium
oxide and intermediate plutonium compounds. The effects of
temperature on reaction kinetics and particle dimensions must
also be understood in order to assess the relevance of
experimental data.

The source term for aerosolization of plutonium oxide is
strongly time-dependent in one case of interest and
independent of time in another. The source term for Pu+O_2
varies with time until a maximum release fraction is reached.
The source term for PuH$_2$+O_2 is virtually independent of time;
the maximum releasable fraction is reached immediately after
exposure to air. If the largest diameter of a releasable
particle is assumed to be 10 μm, the maximum releasable mass
fraction for Pu+O_2 is 0.0007 and that for PuH$_2$+O_2 is 0.25.
The potential for aerosolization of oxide particles from 2.8 g
of plutonium hydride equals the aerosolization potential from
1 kg of plutonium metal.

Size distribution functions are remarkably similar for products of all Pu+gas reactions at high temperatures. The distributions are all bimodal. Marked differences are seen in the sizes of large particles depending on reaction temperature and reaction rate. In contrast, the size distributions of small particles are remarkably similar. The coincidence of sizes in the small particle distribution is attributed to the nature of the stress-induced spallation process for Pu+gas reactions.

Observations made during the evaluation of source-term data are relevant to other safety concerns. Kinetic data for Pu+O$_2$ are essential for assessing the hazard associated with inadvertent exposure of molten plutonium to air during fabrication processes. The oxidation rate of molten metal is much less than predicted by extrapolation of Arrhenius data for solid plutonium. The observed rate (0.2 g PuO$_2$/cm^2 min) is independent of temperature. The maximum temperatures attained during self-sustained burning of kilogram-sized plutonium samples are less than 1000°C.[3] Valuable information related to containment of molten plutonium during a fire are also encountered. The oxide layer formed on the metal apparently provides a containment barrier for molten plutonium and prevents the corrosion of stainless steel at temperatures up to 900°C.[1] This observation suggests that oxidizing environments might enhance the containment capability of steel vessels.

This report provides a new perspective on the aerosolization process for plutonium. Chemical and kinetic factors are identified and their relevance to source-term definition is developed. Several areas requiring further study are recognized. A need is seen for conducting high-temperature containment tests in an oxidizing environment. Issues requiring further definition include the rate and geometry of metal release during containment failure, the oxidation rate of plutonium metal after release and the total size distribution for the high-temperature oxide. These

results will provide a basis for critically evaluating conclusions reached in this report and for addressing additional issues related to definition of the source term.

REFERENCES

1. K. Stewart, "Vixen A Trials: Experiments to Study the Release of Particulate Materials During the Combustion of Plutonium, Uranium and Beryllium in a Petrol Fire," AWRE Report T15/60, Atomic Weapons Research Establishment, Aldermaston, UK, January, 1961.

2. J. Mishima, "Plutonium Release Studies I. Release from the Ignited Metal," USAEC Report BNWL-205, Battelle Pacific Northwest Laboratory, Richland, WA, December 1965.

3. J. Mishima, "Plutonium Release Studies II. Release from Ignited Bulk Metallic Pieces," USAEC Report BNWL-357, Battelle Pacific Northwest Laboratory, Richland, WA, November, 1966.

4. A. F. Edison, H. C. Yeh, and G. M. Kanapilly, _J. Nucl. Mater._, **152**(1988)41.

5. A. F. Edison, H. C. Yeh, and G. M. Kanapilly, "Plutonium Aerosolization Studies," Report SW-331L, Lovelace Inhalation Toxicology Research Institute, Albuquerque, NM, March, 1987.

6. L. A. Mahoney and J. Mishima, "Assessment of the Basis for Modeling Release from Plutonium Oxidation," USDOE Report PNL-SA-18402, Pacific Northwest Laboratory, Richland, WA, August, 1990.

7. F. H. Ellinger, W. N. Miner, D. R. O'Boyle and F. W. Schonfeld, "Constitution of Plutonium Alloys," USAEC Report LA-3870, Los Alamos Scientific Laboratory, Los Alamos, NM, December, 1968.

8. F. L. Oetting, M. H. Rand, and R. J. Ackermann, "The Chemical Thermodynamics of Actinide Elements and Compounds: Part 1 The Actinide Elements," International Atomic Energy Agency, IAEA, Vienna, Austria, 1976.

9. L. R. Morss, "Thermodynamic Properties," in _Chemistry of the Actinide Elements_, 2nd. ed., Vol. 2, Chap. 17, Chapman and Hall, New York, NY, 1986.

10. J. L. Stakebake and L. A. Lewis, _J. Less-Common Met._, **136** (1988)349.

11. H. E. Flowtow, J. M. Haschke, and S. Yamauchi, "The Chemical Thermodynamics of Actinide Elements and Compounds: Part 9 The Actinide Hydrides," International Atomic Energy Agency, IAEA, Vienna, Austria, 1984.

12. J. L. Stakebake and M. R. Dringman, <u>J. Nucl. Mater.</u>, **23** (1967)349.

13. J. M. Haschke, "Actinide Hydrides," in <u>Topics in f-Element Chemistry; Synthesis of Lanthanide and Actinide Compounds</u>, Chap. 1, Reidel-Kluwer Academic Publishers, Dordrecht, Netherlands, 1991.

14. J. L. Stakebake, <u>J. Less-Common Met.</u>, **123**(1986)185.

15. W. N. Miner, A. S. Coffinberry, F. W. Schonfeld, J. T. Waber, R. N. R. Mulford, and R. E. Tate, <u>Rare Metals Handbook</u>, 2nd. ed., Chap. 18, Reinhold Publishing Corp., London, United Kingdom, 1961.

16. J. M. Haschke and S. J. Hale, "Alternative Solvents for Cleaning Plutonium: Thermodynamic and Kinetic Considerations," USDOE Report LA-12255-MS, Los Alamos National Laboratory, Los Alamos, NM, March, 1992.

17. J. L. Stakebake, <u>J. Electrochem. Soc.</u>, **128**(1981)2383.

18. J. L. Stakebake and H. N. Robinson, <u>Nucl. Technol.</u>, **33** (1977)30.

19. J. L. Stakebake, <u>Nucl. Sci. Eng.</u>, **78**(1981)386.

20. J. L. Waber, <u>Plutonium Handbook</u>, Vol. 1, Chap. 6, American Nuclear Society, LaGrange Park, IL, 1980.

21. J. L. Stakebake, EG&G Rocky Flats, Golden, CO, Personal Communication, 1991.

22. J. L. Stakebake and M. A. Saba, <u>J. Less-Common Met.</u>, **158** (1990)221.

23. J. C. Martz, "Dynamics of Metal Etching and Oxidation in Fluorcarbon/Oxygen RF Glow Discharges," Doctoral Dissertation, University of California at Berkeley, Berkeley, CA, 1991.

24. J. M. Haschke, A. E. Hodges, III, and R. L. Lucas, <u>J. Less-Common Met.</u>, **133**(1987)155.

25. R. E. Luna, Sandia National Laboratories, Albuquerque, NM, Personal Communication, 1991.

26. K. Stewart, "The Particulate Material Formed by the Oxidation of Plutonium," in <u>Progress in Nuclear Energy</u>, Pergamon Press, New York, NY, 1963.

Table I. Kinetic and Particle Collection Data for the $Pu+O_2$ Reaction

Ref.	Pu Sample			Reaction				Particle Collection		
	Starting phase	mass (g)	area (cm^2)	Temp. (°C)	Time (min)	%	rate[a]	mass (g)	time (min)	released fraction
1	α	203	41	860±40	23±7	43	12±5	0.2[b]	---	0.023
1	α	202	41	500±40	60±20	100	11±7	1.7[b]	---	0.0084
3	α	568	68	900±50	30±5	100	37±12	0.27[c]	90	0.00047
3	α	1770	188	925±50	55±5	100	27±10	0.29[c]	45	0.00020[d]
3	δ	997	140	775±50	75±5	100	13±9	0.04[c]	22	0.00013[d]

a.   Rate in mgO_2/cm^2 min.

b.   Particle mass reported for integrated deposition contours.

c.   Mass converted to grams of PuO_2 collected.

d.   Released fractions based on 80% completion of oxidation during 45 min collection time and 30% completion of oxidation during 22 min collection time.

Table II. Size Distribution for Pu Powder Prepared by Hydriding Massive Pu and Thermally Decomposing the Hydride Product in Dynamic Vacuum. Data obtained from the particle distribution reported by Stakebake.[17]

Particle Diameter[a] (μm)	Cumulative Particle Fraction	Cumulative Mass Fraction[b]
1.5	0.32	4.9×10^{-7}
3.0	0.48	4.3×10^{-5}
5.0	0.50	1.1×10^{-4}
8.0	0.60	5.2×10^{-4}
15	0.68	2.3×10^{-3}
30	0.78	0.018
50	0.83	0.081
70	0.89	0.22
85	0.95	0.53
95	0.98	0.80
100	>0.99	0.99

a. Particle diameters are geometric, not aerodynamic.

b. Mass distribution calculated for spherical particles of stated diameters using 10.45 g/cm^3 for the PuH$_2$ density.

Table III. Size Distribution for PuO_2 Prepared by High Temperature Oxidation of Pu in Air. Combined data from Stewart,[1] Stakebake,[17] and Mishima.[3]

Particle Diameter[a] (μm)	Mass Distribution		Particle Distribution[b]	
	corresponding mass fraction	cumulative mass fraction	corresponding particle fraction	cumulative particle fraction
0.25	3.8×10^{-9}	3.8×10^{-9}	0.124	0.12
0.35	9.1×10^{-9}	1.3×10^{-8}	0.110	0.23
0.50	6.7×10^{-8}	8.0×10^{-8}	0.069	0.30
1.5	4.2×10^{-7}	5.0×10^{-7}	0.110	0.41
3.0	4.5×10^{-5}	4.6×10^{-5}	0.204	0.62
5.0	6.4×10^{-5}	1.1×10^{-4}	0.063	0.68
8.0	4.2×10^{-4}	5.3×10^{-4}	0.102	0.78
15	1.9×10^{-3}	2.4×10^{-3}	0.124	0.91
30	1.7×10^{-2}	1.9×10^{-2}	0.080	0.99
52	8.4×10^{-3}	2.7×10^{-2}	7.3×10^{-3}	>0.99
77	1.1×10^{-2}	3.9×10^{-2}	3.8×10^{-3}	
150	9.2×10^{-2}	0.13	3.2×10^{-3}	
300	0.155	0.29	7.1×10^{-4}	
600	0.263	0.55	1.5×10^{-4}	
1000	0.223	0.77	2.8×10^{-5}	
1700	0.217	0.99	5.5×10^{-6}	
2500	4.9×10^{-3}	0.99+	3.8×10^{-8}	
3000	6.8×10^{-3}	~1.00	2.3×10^{-8}	

a. Particle diameters are geometric, not aerodynamic.

b. Particle distribution based on spherical particles of stated diameters and 11.45 g/cm^3 for the PuO_2 density.

Table IV.   Size Distribution for PuO_2 Prepared by High Temperature Oxidation of PuH_2 in Air. Values derived from data by Stakebake and Robinson.[18]

Particle Diameter[a] (μm)	Mass Distribution		Particle Distribution[b]	
	corresponding mass fraction	cumulative mass fraction	corresponding particle fraction	cumulative particle fraction
0.25	2.4×10^{-7}	2.4×10^{-7}	0.02	0.02
0.35	9.4×10^{-7}	1.2×10^{-6}	0.03	0.05
0.50	1.6×10^{-5}	1.7×10^{-5}	0.04	0.09
1.5	5.8×10^{-4}	6.0×10^{-4}	0.41	0.50
3.0	0.018	0.02	0.22	0.72
5.0	0.063	0.08	0.16	0.88
8.0	0.110	0.19	0.07	0.95
15	0.220	0.41	0.037	0.987
20	0.178	0.59	0.007	0.994
25	0.147	0.74	0.003	0.997
30	0.084	0.82	0.001	0.998
35	0.131	0.95	0.001	0.999
45	0.036	0.99	0.0001	0.9999

a.   Particle diameters are geometric, not aerodynamic.

b.   Mass distribution calculated for spherical oxide particles 11.45 g/cm^3 for the PuO_2 density.

Table V.   Size Distribution Obtained for PuO_2 Using a Fracture Model to Calculate the Particle Redistribution During PuH_2 Oxidation.

Particle Diameter[a] (μm)	Mass Distribution		Particle Distribution[b]	
	corresponding mass fraction	cumulative mass fraction	corresponding particle fraction	cumulative particle fraction
0.5	7.2×10^{-6}	7.2×10^{-6}	0.075	0.08
1.5	2.4×10^{-4}	2.5×10^{-4}	0.383	0.46
3.0	2.3×10^{-3}	2.5×10^{-3}	0.112	0.57
5.0	1.1×10^{-2}	1.5×10^{-2}	0.122	0.68
8.0	7.2×10^{-2}	8.7×10^{-2}	0.187	0.87
15	0.130	0.22	0.051	0.92
20	0.139	0.36	0.027	0.95
25	0.335	0.69	0.028	0.98
30	0.288	0.98	0.014	0.99
35	2.2×10^{-2}	~1.00	6.6×10^{-4}	~1.00

a. Particle diameters are geometric, not aerodynamic.

b. Particle distribution calculated for spherical oxide particles with 11.45 g/cm^3 for the PuO_2 density.
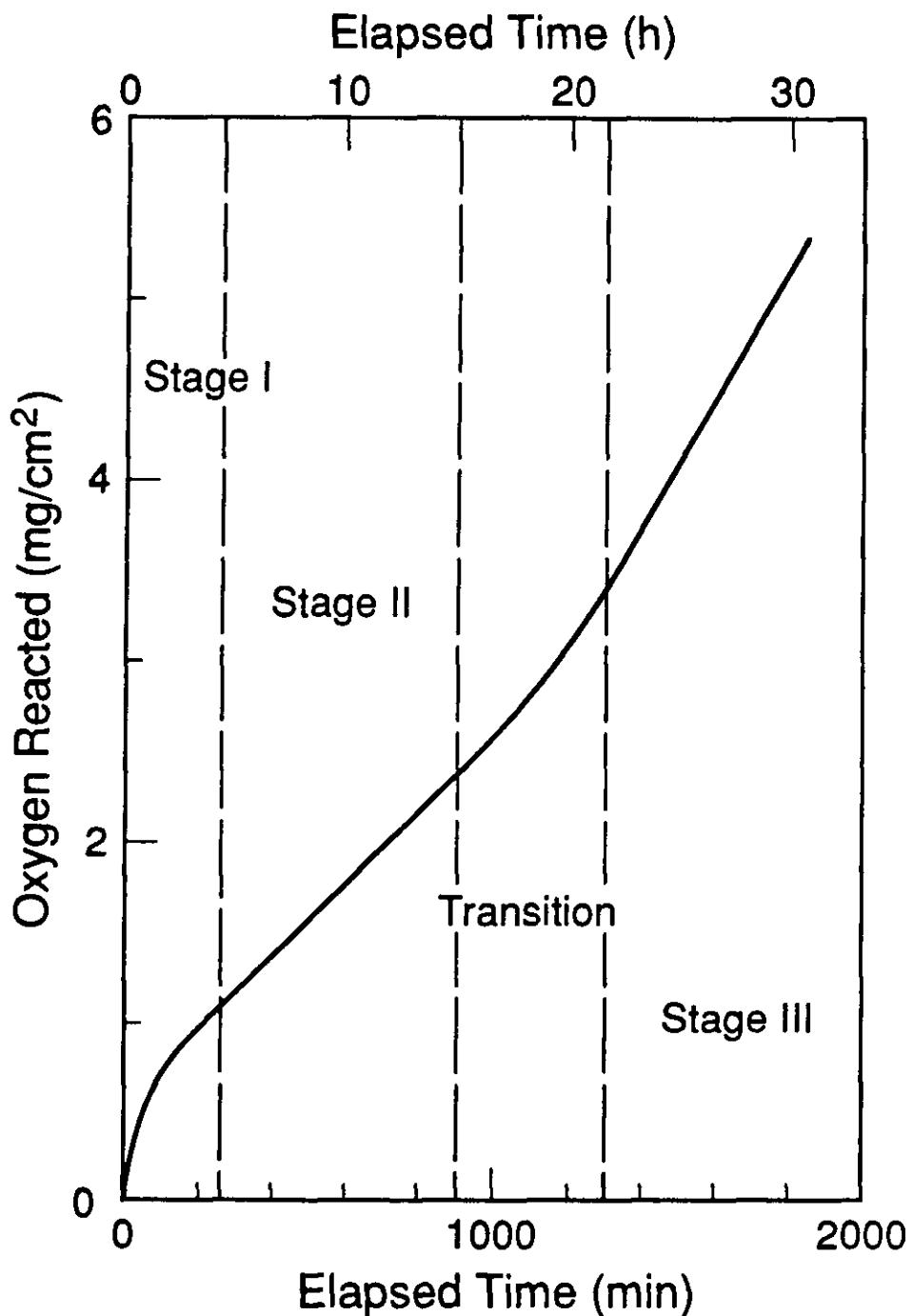
Figure 1.   The stages of reaction observed for oxidation of plutonium metal. The curve is based on data for the Pu+O₂ reaction at 300°C and 1 torr O₂ pressure.[10]
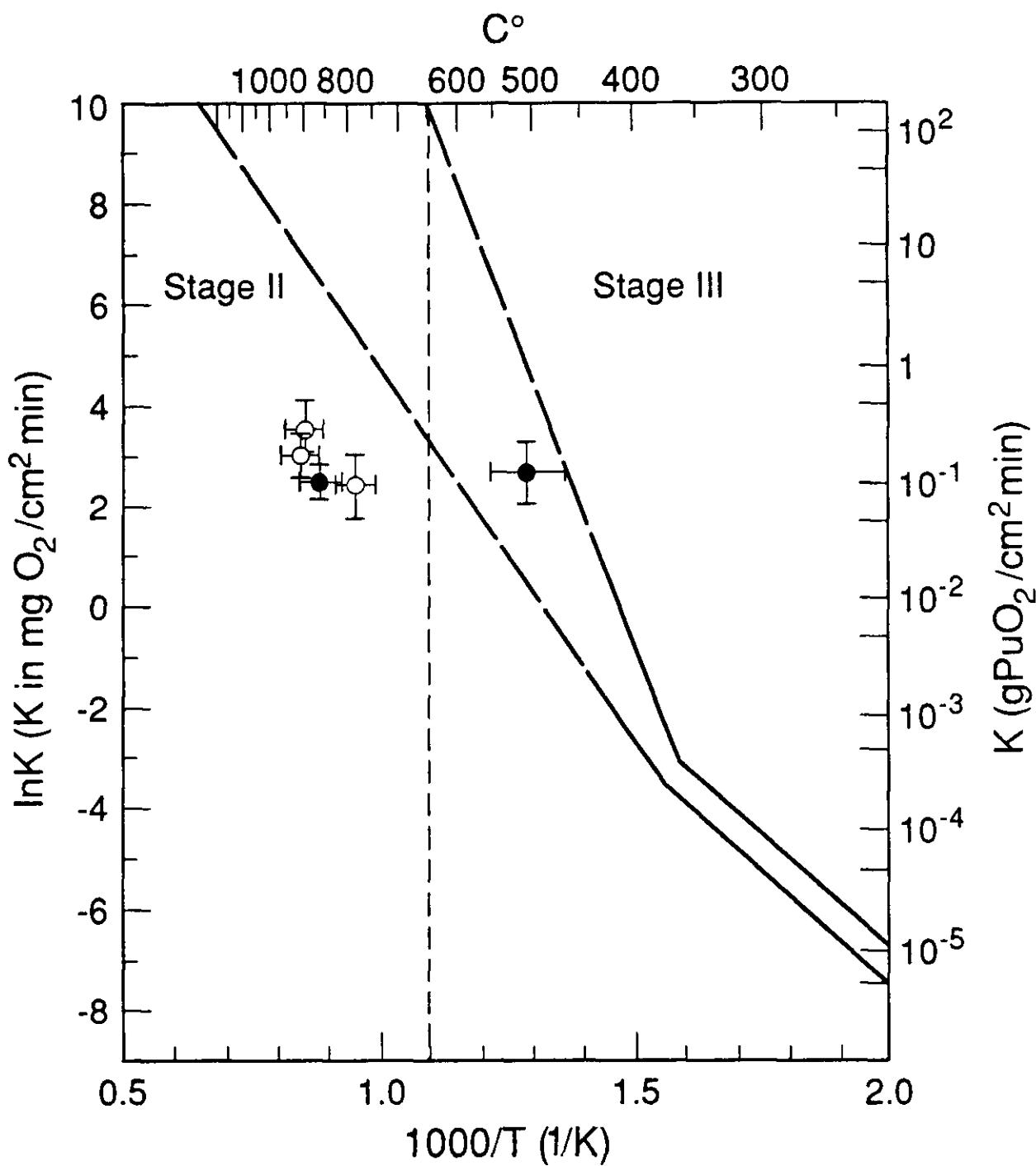
Figure 2. The temperature dependence of the oxidation rate for Pu+O$_2$. Arrhenius curves are from kinetic measurements by Stakebake[10]; rates shown by solid and open symbols are derived from data of Stewart[1] and Mishima,[3] respectively.
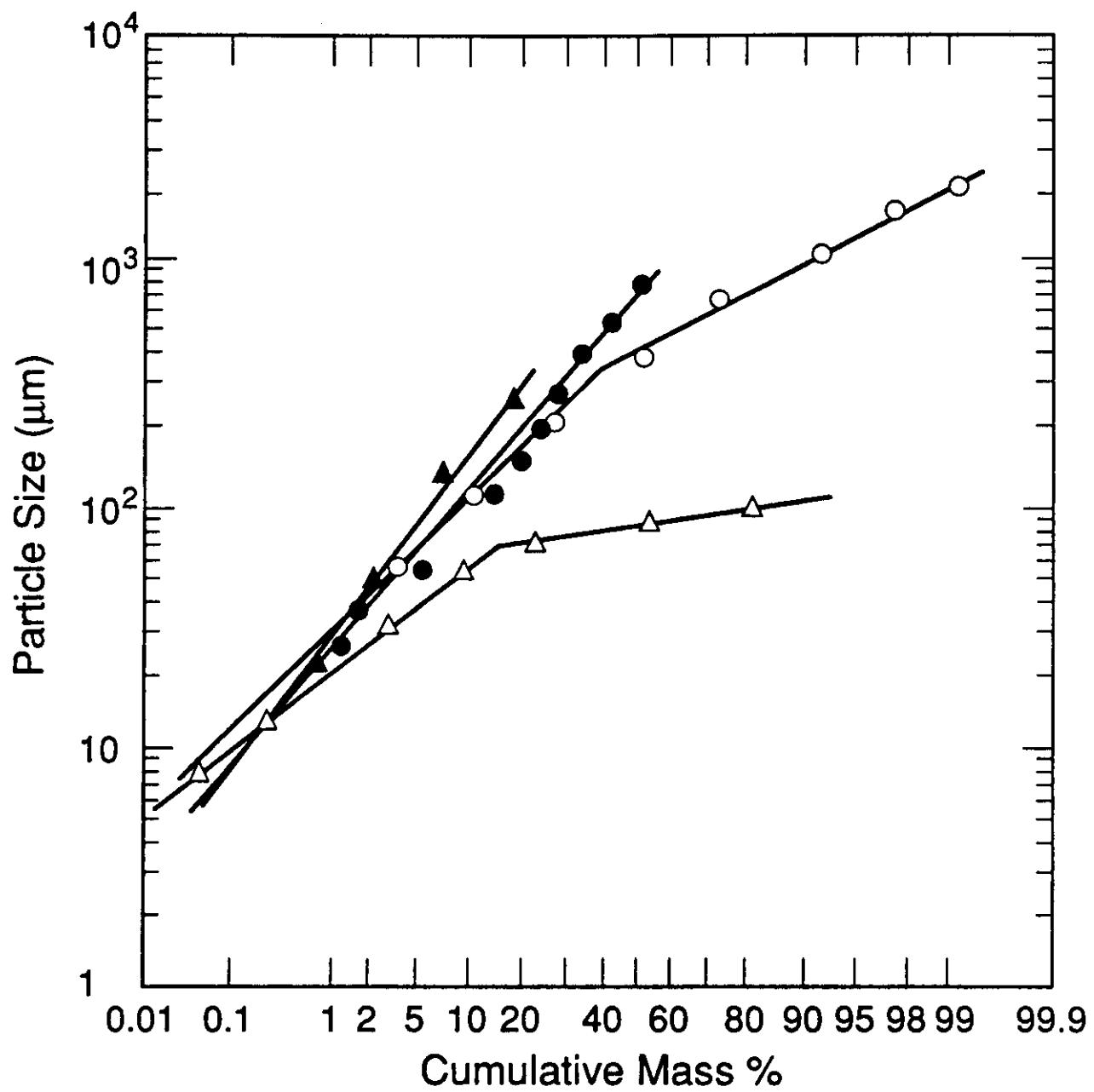
Figure 3.   Cumulative mass distribution for large product
             particles of Pu+gas reactions.   Data for high-
             temperature PuO_2 are shown by circles[1] and solid
             triangles[2]; data for PuH_2 are shown by open
             triangles.[17]
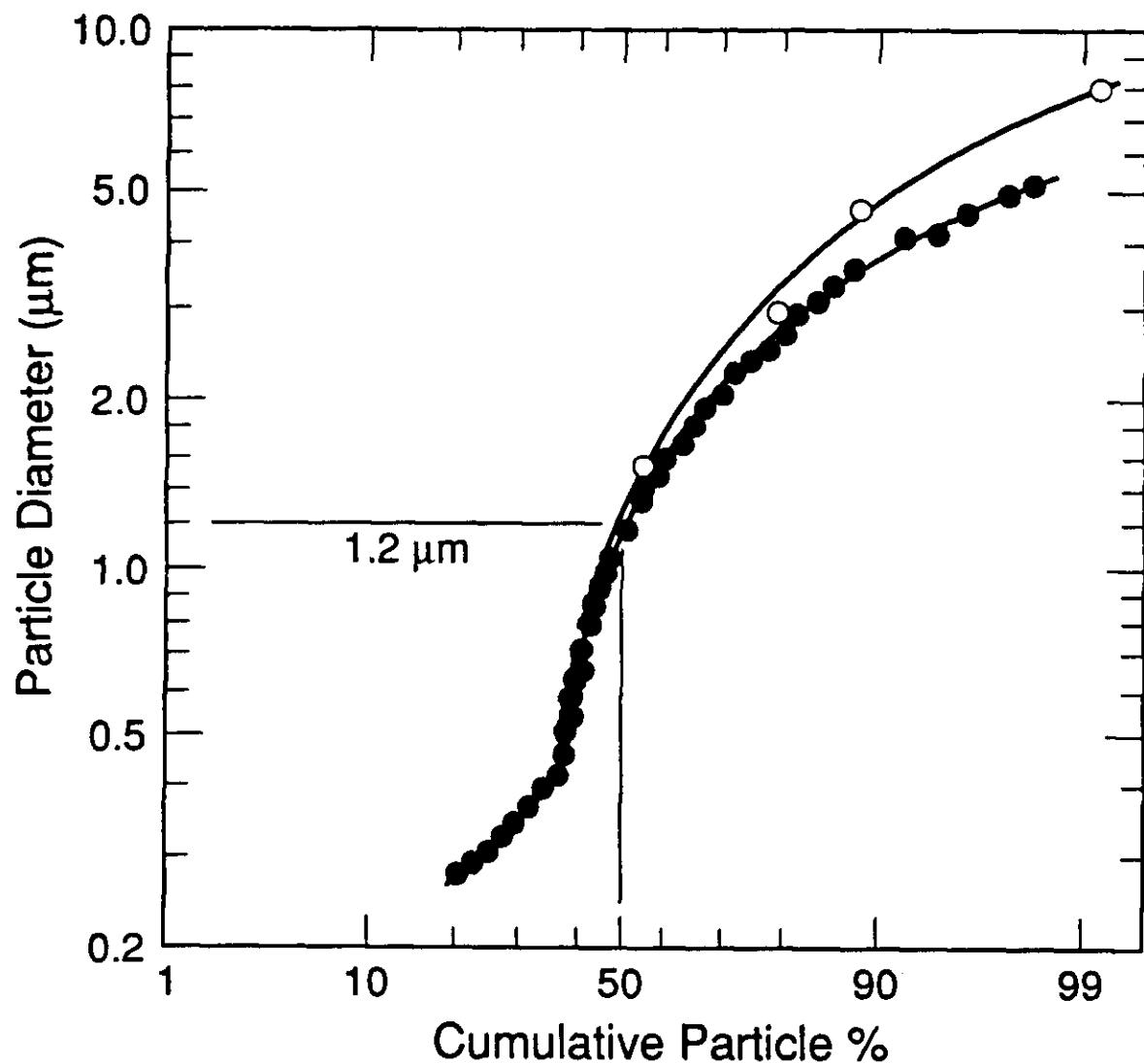
Figure 4.   Cumulative particle distributions for small product
             particles of Pu+gas reactions. Data for entrained
             PuO$_2$ are shown by solid circles[3]; data for PuH$_2$
             particles < 10 μm are shown by open circles.[17]
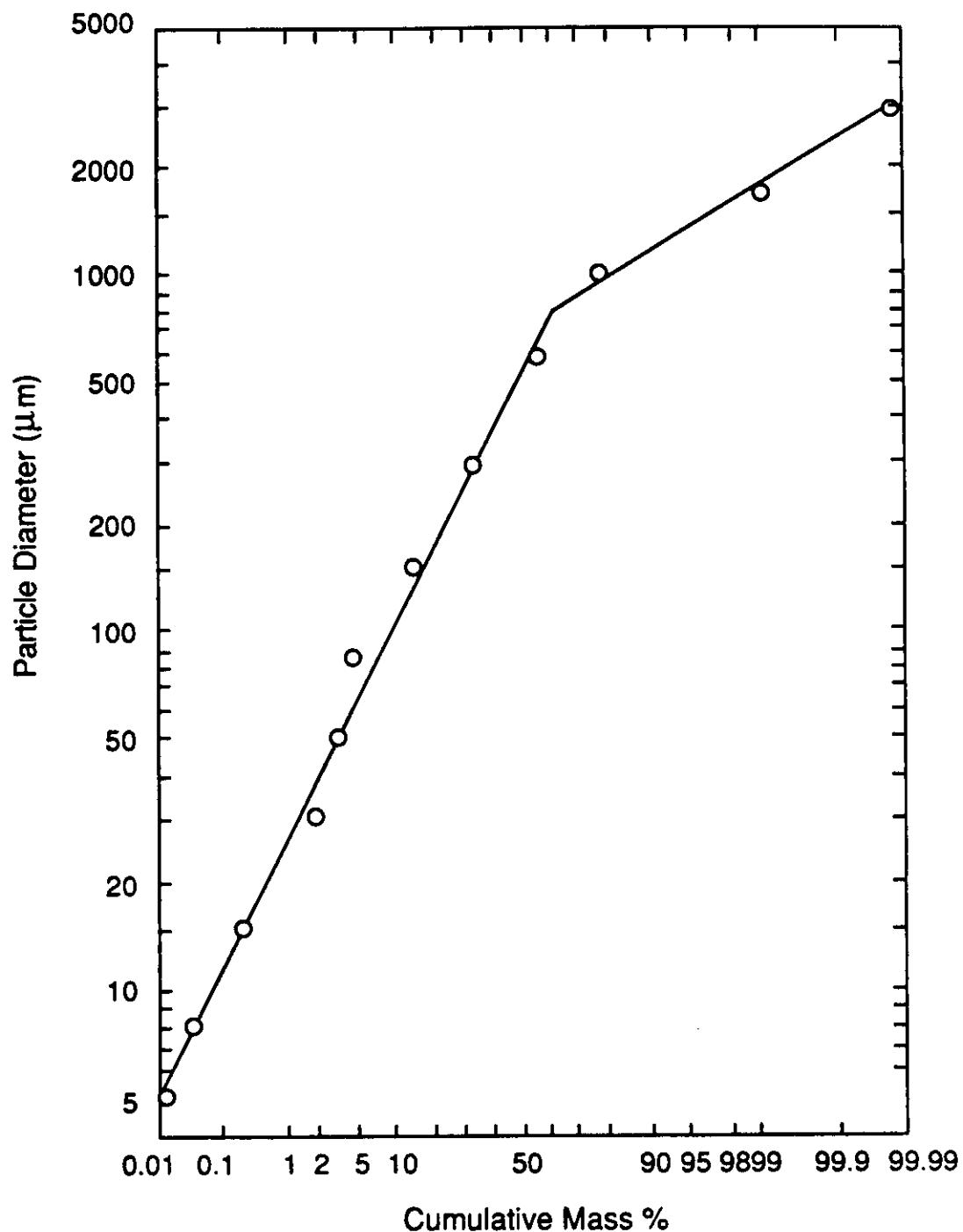
Figure 5. The cumulative mass distribution derived for oxide formed by the Pu+O$_2$ reaction at temperatures above 500°C.
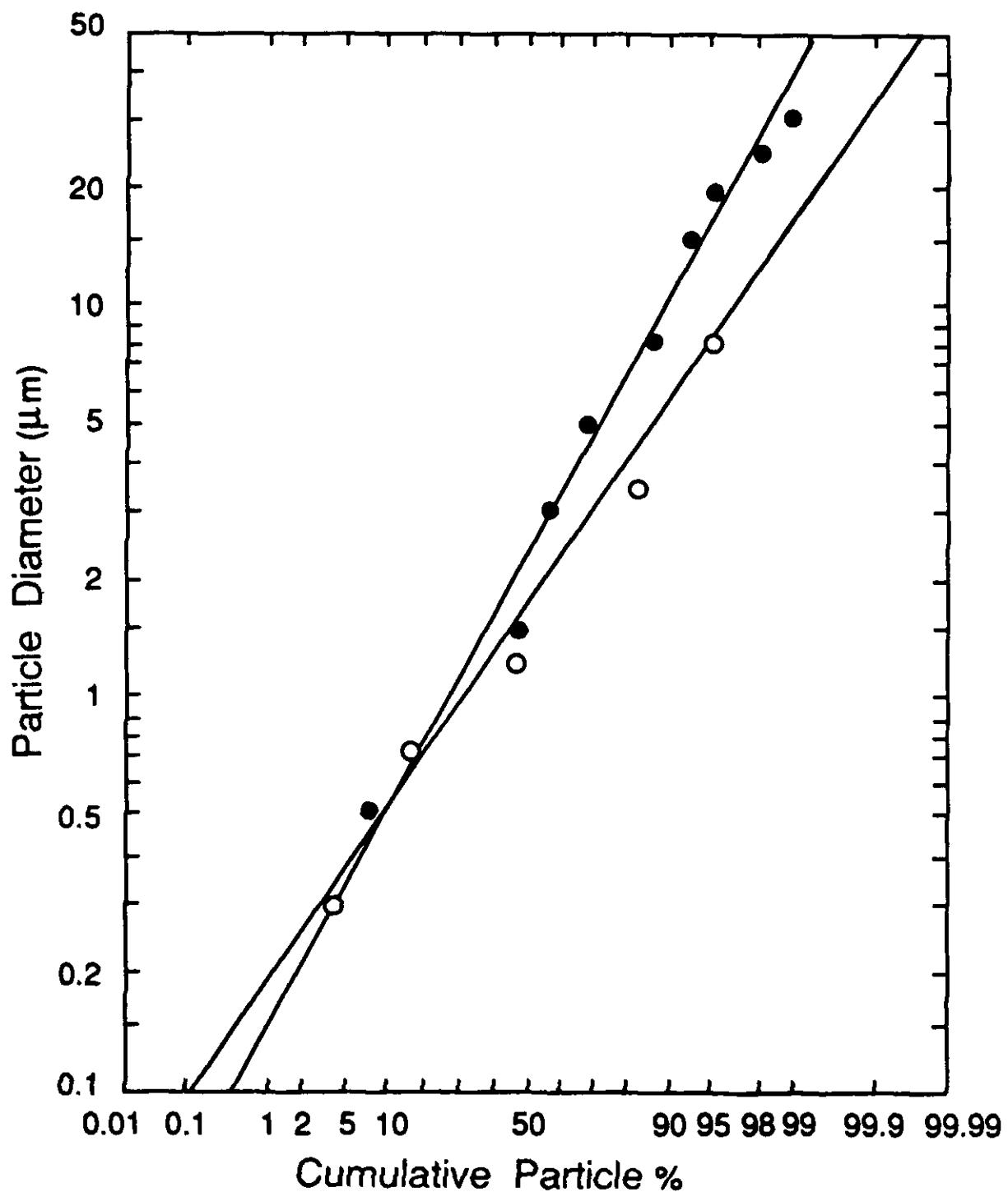
Figure 6. Comparison of cumulative particle distributions for oxide formed by the PuH_2+O_2 reaction. Experimental data from Stakebake and Robinson[18] are shown by open symbols; values predicted using the fracture model are shown by solid symbols.
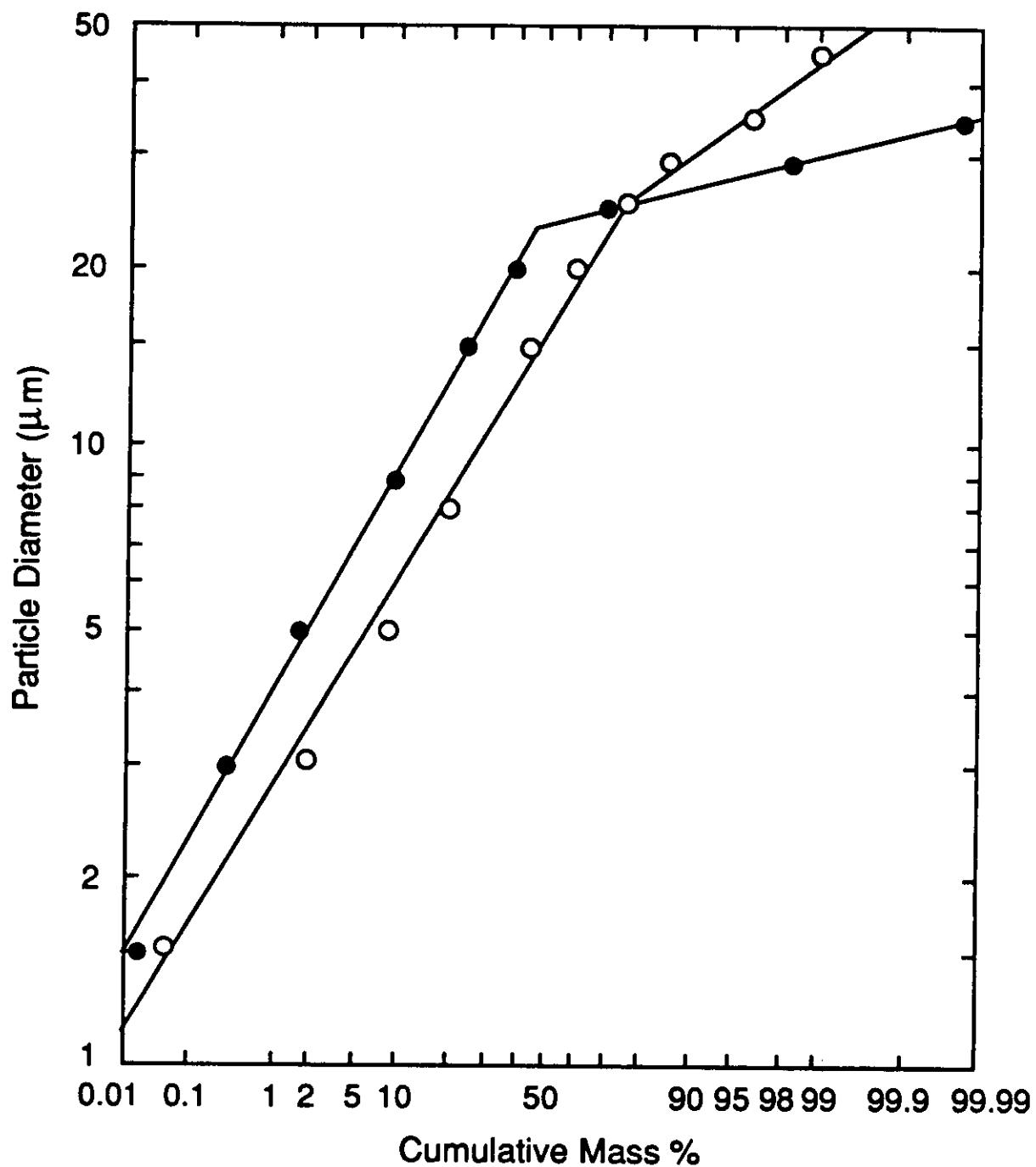
Figure 7.   Comparison of cumulative mass distributions for oxide formed by the PuH_2+O_2 reaction. Experimental data from Stakebake and Robinson[18] are shown by open symbols; values predicted using the fracture model are shown by solid symbols.
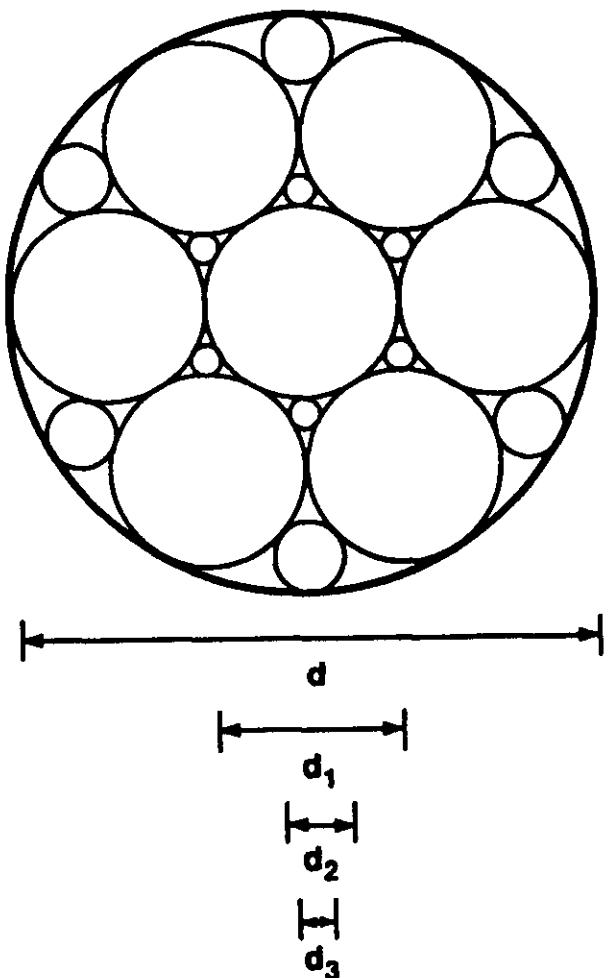
Figure 8.   Closest-packed planar array of spherical product
            particles with diameters d_1, d_2 and d_3 formed by
   fracture of a spherical reactant particle with
            diameter d.
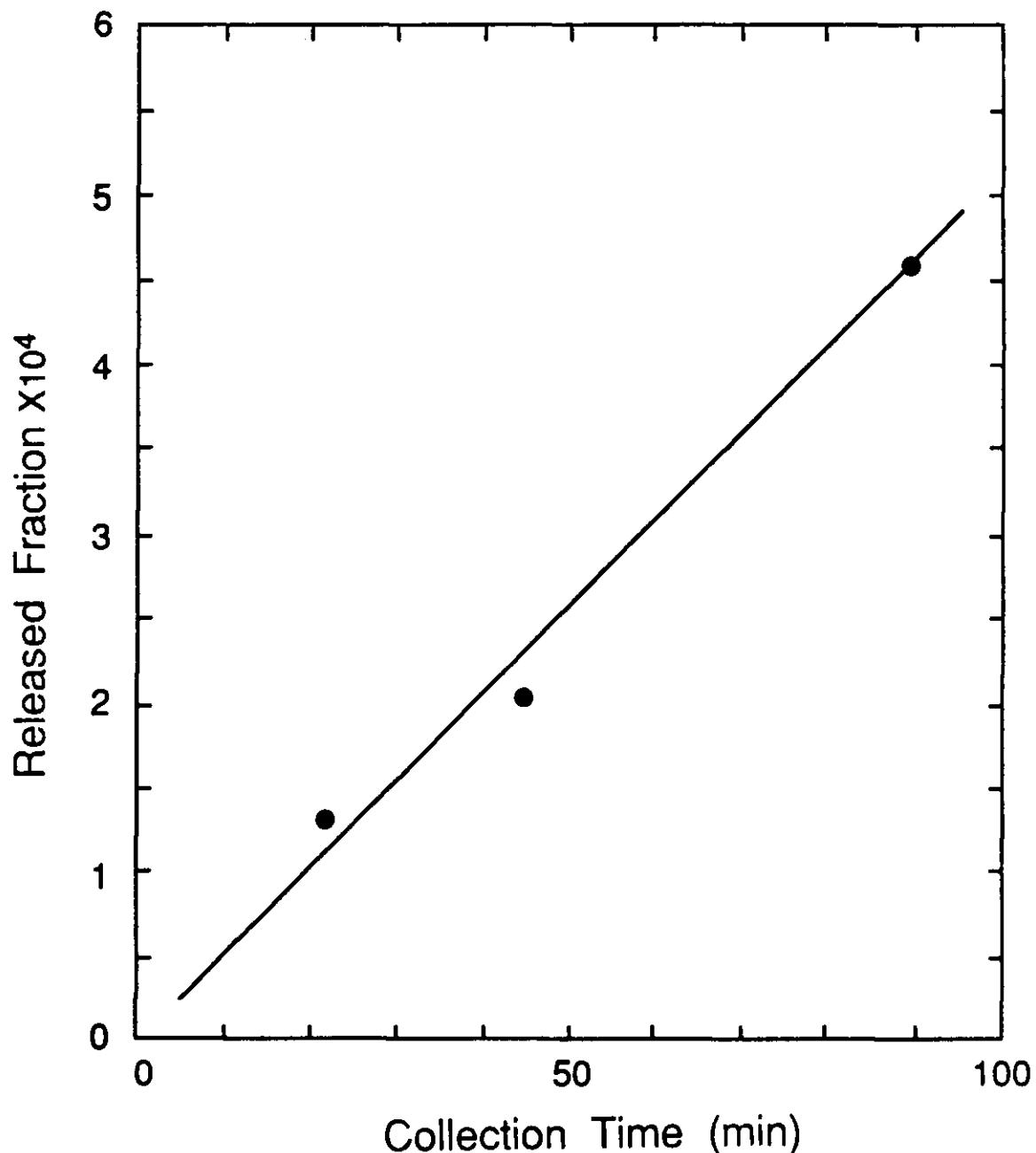
Figure 9. Dependence of the released fraction of PuO_2 particles on the collection time.

Los Alamos Los Alamos National Laboratory
Los Alamos, New Mexico 87545